Electron affinity of cubic boron nitride terminated with vanadium oxide

Yu Yang, Tianyin Sun, Joseph Shammas, et al.

View Online   Export Citation   CrossMark

ARTICLES YOU MAY BE INTERESTED IN

Electron affinity of cubic boron nitride terminated with vanadium oxide

Yu Yang,[1] Tianyin Sun,[1] Joseph Shammas,[1] Manpuneet Kaur,[2] Mei Hao,[1] and Robert J. Nemanich[1]

[1]*Department of Physics, Arizona State University, Tempe, Arizona 85287-1504, USA*
[2]*School for Engineering of Matter, Transport and Energy, Arizona State University, Tempe, Arizona 85287-6106, USA*

A thermally stable negative electron affinity (NEA) for a cubic boron nitride (c-BN) surface with vanadium-oxide-termination is achieved, and its electronic structure was analyzed with *in-situ* photoelectron spectroscopy. The c-BN films were prepared by electron cyclotron resonance plasma-enhanced chemical vapor deposition employing BF_3 and N_2 as precursors. Vanadium layers of ∼0.1 and 0.5 nm thickness were deposited on the c-BN surface in an electron beam deposition system. Oxidation of the metal layer was achieved by an oxygen plasma treatment. After 650 °C thermal annealing, the vanadium oxide on the c-BN surface was determined to be VO_2, and the surfaces were found to be thermally stable, exhibiting an NEA. In comparison, the oxygen-terminated c-BN surface, where B_2O_3 was detected, showed a positive electron affinity of ∼1.2 eV. The B_2O_3 evidently acts as a negatively charged layer introducing a surface dipole directed into the c-BN. Through the interaction of VO_2 with the B_2O_3 layer, a B-O-V layer structure would contribute a dipole between the O and V layers with the positive side facing vacuum. The lower enthalpy of formation for B_2O_3 is favorable for the formation of the B-O-V layer structure, which provides a thermally stable surface dipole and an NEA surface. © *2015 AIP Publishing LLC*. [http://dx.doi.org/10.1063/1.4934508]

I. INTRODUCTION

A number of wide band gap semiconductors (diamond, boron nitride, aluminum nitride, etc.) have attracted research interest for electron emission applications because of their abilities to exhibit a low or negative electron affinity (NEA). For NEA materials, the vacuum level lies below the conduction band minimum (CBM). Electrons can leave an NEA surface without encountering a barrier, leading to a strong emissivity.

In the case of diamond, a wide band gap material with $E_G \sim 5.5$ eV, an NEA can be readily achieved with hydrogen-termination.[1–3] Recently, nitrogen- and phosphorus-doped NEA diamond films have shown a low effective work function, enabling thermionic electron emission at or below 500 °C, which leads to promising applications in thermionic and photon-enhanced thermionic energy conversion (TEC) devices.[4–6] Cubic boron nitride (c-BN) has a wide band gap of ∼6.1–6.4 eV,[7–9] is isoelectronic to diamond, and owns similar properties to various aspects of diamond. The hydrogen-terminated c-BN surface has also been reported to exhibit an NEA.[9–12] Our group has successfully employed plasma-enhanced chemical vapor deposition (PECVD) with fluorine chemistry to prepare c-BN films, which could serve as an alternative material for energy-related applications.[9]

For TECs, a high operation temperature is desired for high conversion efficiency, yet desorption of hydrogen from the diamond and c-BN surfaces at temperatures above 800 °C has limited the performance of TECs based on these NEA materials.[3,11,12] In addition, the hydrogen-termination surface is more easily destroyed by annealing in the air, or with an oxygen plasma or other oxidation processes.[13–15] It is therefore worthwhile to investigate alternative surface termination approaches for providing a more thermally stable NEA. Metal oxides have been reported to induce an NEA on materials such as GaAs[16] and diamond.[17–20] Recently, theoretical and experimental studies have indicated that transition metal oxides are stable and can significantly influence the electronic properties of diamond.[21] However, there have been few reports of experimental results of similar effects on c-BN. Vanadium oxide (VO_2) is a narrow band gap material ($Eg = 0.7$ eV).[22] For metal oxide coatings with the same electron affinity, a smaller band gap will more likely lead to an effective NEA. And for small band gap materials such as VO_2, the electrons emitted from c-BN can be transmitted through real states, instead of tunneling through in-gap states. Vanadium oxides have also attracted interest for their moderate temperature insulator-to-metal transition (IMT)[23,24] and are considered for applications in electronic and optoelectronic devices. We have obtained preliminary results indicating that vanadium-oxide-termination of boron-doped diamond surfaces exhibit an NEA.[25] These results have motivated us to investigate how the vanadium-oxide-termination changes the electron affinity of the c-BN surface where we have employed *in-situ* photoelectron spectroscopy to establish the electronic properties of the surfaces after various processing steps.

II. EXPERIMENT

The vanadium-oxide-termination was achieved with two approaches. One was to deposit a thin layer of vanadium metal on the c-BN film, which was followed by an oxygen plasma process to oxidize the film. Samples obtained from

this approach are labeled as BN-1. The second method involved terminating the c-BN films with oxygen first, and then depositing the vanadium layer. Samples processed in this way are labeled as BN-2 and BN-3.

The experiments were accomplished *in situ* in an integrated ultrahigh vacuum (UHV) system which was maintained at a base pressure of $\sim 1 \times 10^{-9}$ Torr. In this UHV system, different processing and characterization chambers are connected by an ~ 20 m long linear transfer line. The systems utilized in the experiments were as follows: an electron cyclotron resonance (ECR) PECVD system for deposition of the c-BN films, a reactive electron beam deposition system for deposition of the vanadium films, a remote oxygen plasma system for oxidation of the vanadium layers and the c-BN surfaces, an X-ray photoelectron spectroscopy (XPS) system for core level analysis, and an ultraviolet photoelectron spectroscopy (UPS) system for characterization of the electronic structure of the sample.

The c-BN films were prepared in the ECR-PECVD system employing fluorine chemistry.[9] The substrates were 25 mm diameter, heavily phosphorus-doped ($[P] > 10^{19}$ cm^{-3}), single side polished silicon (100) wafers. Before deposition, the sample underwent a 15 min *in-situ* plasma cleaning process at 780 °C, which employed a He-Ar-N_2 gas mixture, with flow rates of 35, 2.5, and 12.5 standard cubic centimeters per minute (sccm), respectively, a microwave input of 1.4 kW, and an applied bias of -60 V. The deposition process was initiated by introducing H_2 and BF_3 at flow rates of 1 and 4 sccm, respectively, into the He-Ar-N_2 gas mixture with the same parameters of bias, temperature, and input power. The deposition process lasted for approximately 4 h and resulted in BN films of $\sim 0.1 \mu$m thick.

The vanadium films were deposited using a reactive electron beam deposition system, with vanadium metal of 99.8% purity and an alumina crucible. Vanadium films with thickness of ~ 0.1 nm for samples BN-1 and BN-2, or ~ 0.5 nm for BN-3, were deposited on the c-BN sample at ambient temperature and an oxygen chamber pressure of $\sim 1 \times 10^{-7}$ Torr. A growth rate of ~ 0.01 nm/s was obtained, which was monitored and maintained by a quartz crystal microbalance (QCM).

Oxidation of the metal layer and formation of the O-termination on c-BN films were achieved using an oxygen plasma treatment. The remote plasma was generated by 30 W of RF excitation with the sample at ambient temperature. The 100 mTorr oxygen pressure was maintained with a gas flow rate of 30 sccm. The oxidation process lasted for ~ 1 min.

In order to remove excess oxygen from the sample surface, a 30 min 650 °C UHV annealing process was initiated using a tungsten irradiation heater coil beneath the sample holder. The temperature of the sample was controlled by a thermocouple positioned behind the center of the sample and calibrated with a Mikron M90Q infrared pyrometer.

After each processing step, samples were characterized by *in-situ* XPS and UPS. The XPS analysis was performed using the 1486.6 eV Al Kα line of a VG XR3E2 dual anode source (Mg and Al) and a VG microtech Clam II analyzer. The analyzer was operated at a pass energy of 20 eV and a

resolution of ~ 1.0 eV. The binding energy position of the core levels can be further resolved to $\sim \pm 0.1$ eV by curve fitting the core level peaks. The XPS was calibrated with a standard gold foil, by aligning the Au 4f$_{7/2}$ peak to 84.0 eV.

The UPS spectra were obtained using a system equipped with a VSW HA50 hemispherical analyzer and VSW HAC300 controller, operated at a pass energy of 15 eV, giving a resolution of ~ 0.15 eV. The photon source was optimized for He I radiation (h$\nu = 21.2$ eV), which is generated from a He discharge lamp operated at ~ 600 V with a discharge current of 200 mA. A -8.0 V bias was applied to the substrate to overcome the work function of the analyzer. To avoid photo-induced charging, the samples were heated to ~ 280 °C, which was controlled by a thermocouple behind the sample. The UPS system was calibrated against a gold foil, and the Fermi level was regarded as the reference energy.

III. RESULTS

A. Cubic BN with O-termination

As a control experiment, a c-BN film deposited under the same conditions was treated with an oxygen plasma and annealed at 650 °C. XPS and UPS results from the control experiment are shown in Fig. 1. Gaussian curve fitting was employed to determine the positions of the XPS peaks. After oxygen plasma treatment, the O 1s signal increased significantly, indicating the c-BN surface had adsorbed oxygen. The B 1s peak shifted 0.6 eV towards lower binding energy, from 191.6 ± 0.1 eV to 191.0 ± 0.1 eV, while the N 1s core level shifted from 399.1 ± 0.1 eV to 398.6 ± 0.1 eV. The shift of the N 1s peak corresponded to the shift of the B 1s peak within the resolution of the XPS system. The 30 min 650 °C annealing process restored the B and N 1s core levels to the positions before oxidation. After annealing, the O 1s peak shifted 0.7 eV to a higher binding energy of 532.9 eV, which is consistent with the reported value for B_2O_3.[26]

The c-BN surface is presumed to be hydrogen-terminated after the ECR-PECVD deposition.[9] The UPS scans of as-grown c-BN showed a 1.7 eV front cutoff and 16.5 eV back cutoff (relative to the Fermi level). With a He I photon energy of 21.2 eV, the CBM position for hydrogen-terminated c-BN was deduced to be 4.7 eV. The sum of the CBM 4.7 ± 0.15 eV and valence band maximum (VBM) 1.7 ± 0.15 eV relative to the Fermi level is $\sim 6.4 \pm 0.2$ eV, which is within the reported range of the c-BN band gap. This result indicates that the as-grown c-BN likely exhibited an NEA. The oxidation process increased the c-BN work function to 5.7 eV, and the VBM shifted to 2.5 eV below the Fermi level. The spectral width is ~ 14.8 eV, indicating that O-terminated c-BN exhibits a positive electron affinity (PEA).[27] While the annealing process was able to reduce the work function to a lower value of ~ 5.2 eV, combined with the VBM position which is at 2.4 eV, the results still suggest that the c-BN exhibits a PEA before and after annealing. By applying the same band gap of 6.4 eV, a PEA of 1.2 ± 0.2 eV was deduced for the O-terminated c-BN films.
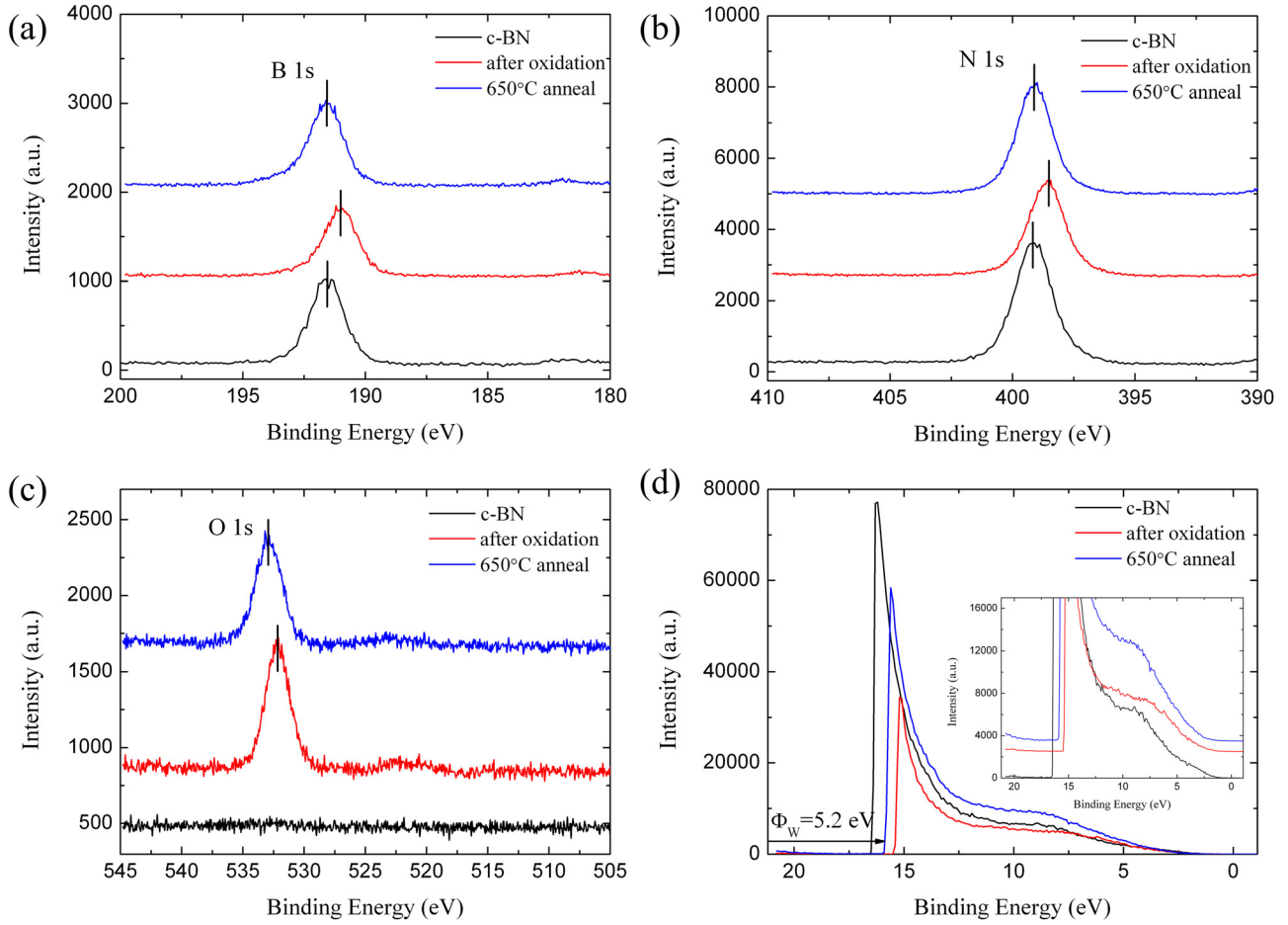
FIG. 1. XPS scans of the O-terminated c-BN sample, showing the (a) B 1s, (b) N 1s, (c) O 1s core level peaks, and (d) the UPS SCANS. The work function variations are indicated in the UPS scans.

The measured binding energies of the B 1s, N 1s, O 1s core levels, the work function, and the VBM for the O-terminated c-BN film are summarized in Table I.

B. BN-1

XPS and UPS scans after each preparation step for sample BN-1 are shown in Fig. 2. The deposition of vanadium films on the c-BN surface did not lead to a change in the positions of the B and N core levels. After vanadium deposition, the V $2p_{3/2}$ core level could be clearly observed at a binding energy of 516.4 eV, indicating that a vanadium layer was successfully formed on the c-BN surface. A small amount of oxygen was incorporated during vanadium deposition due to the oxygen background in the chamber, which is more significant for the very thin layer deposition. After plasma oxidation, the B 1s peak shifted 0.7 eV towards lower binding energy, and the N 1s peak exhibited a similar shift.

TABLE I. B 1s, N 1s, O 1s core levels, effective work function (Φ_W), and VBM for O-terminated c-BN relative to the Fermi level, in eV.

Process	B 1s	N 1s	O 1s	Φ_W	VBM
H-termination	191.6	399.1	…	4.7	1.7
Oxidation	191.0	398.6	532.2	5.7	2.5
650 °C annealing	191.6	399.1	532.9	5.2	2.4

Compared with O-terminated c-BN, the vanadium deposition and oxidation appeared to affect the B and N core levels differently from the V core level. The V $2p_{3/2}$ core level shifted 1.1 eV to higher binding energy, while the O 1s peak was observed at a lower binding energy of 531.4 eV, resulting in a reduction of $\sim$1.7 eV in the V-O binding energy difference. The annealing process restored the B and N peaks to the original positions. The vanadium peak was determined to be at 516.9 eV, and the binding energy of the O 1s core level increased by 1.3 eV to 532.7 eV, resulting in an $\sim$1.9 eV increase of the V-O binding energy difference.

After the vanadium deposition, the back cutoff of the spectrum was at 16.8 eV. Combined with the photon energy of 21.2 eV, the work function of the surface corresponded to the work function of vanadium ($\Phi_W = 4.3$ eV (Ref. 28)) or the work function of V_2O_3 ($\Phi_W = 4.4$ eV (Ref. 29)) within the experimental uncertainty. An oxygen plasma treatment has been reported to increase the work function of diamond surfaces.[30] This was also observed in this experiment. The back cutoff of the UV-photoemission spectra shifted 1.6 eV to lower binding energy after exposure to an O-plasma, corresponding to an increase of the work function. Annealing at 650 °C in UHV reduced the surface work function by $\sim$1.0 eV. With the band gap of $\sim$6.1–6.4 eV for c-BN, the spectral width, which is $\sim$15.1 eV, implies that BN-1 exhibits an NEA.[27]
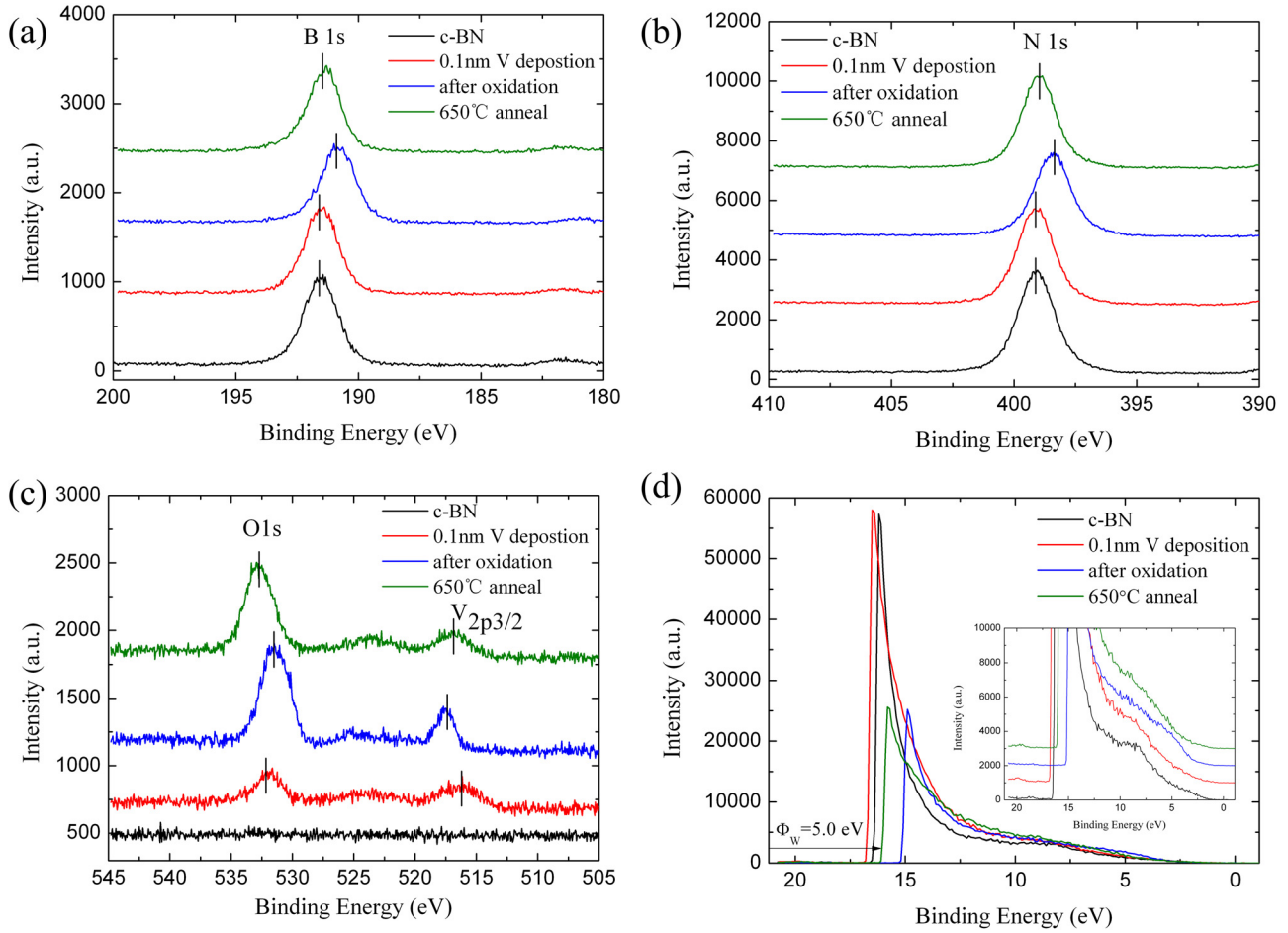
FIG. 2. XPS scans of the BN-1 sample, showing the (a) B 1s, (b) N 1s, (c) O 1s core level peaks, and (d) the UPS scans.

The measured binding energies of the B 1s, N 1s, O 1s, and V $2p_{3/2}$ core levels, the work function, and the VBM of BN-1 are summarized in Table II.

C. BN-2

Spectroscopic results from sample BN-2 are shown in Fig. 3. After oxidation, the B and N 1s core levels were observed to shift towards lower binding energy by 0.4 eV. The deposition of the vanadium layer restored the positions of the B and N 1s peaks, and significantly reduced the work function from 6.2 eV to 4.5 eV. Similar to sample BN-1, thermal annealing changed the binding energy difference between the V and O core levels, indicating a change in the vanadium-oxide bonding. The final position of the O 1s is the same as that of BN-1, while the final binding energy of the V $2p_{3/2}$ core level is 0.3 eV higher.

TABLE II. B 1s, N 1s, O 1s, V $2p_{3/2}$ core levels, effective work function (Φ_W), and VBM for BN-1 relative to the Fermi level, in eV.

Process	B 1s	N 1s	O 1s	V $2p_{3/2}$	Φ_W	VBM
H-termination	191.5	399.1	…	…	4.7	1.6
Vanadium deposition	191.5	399.1	532.0	516.4	4.4	1.8
Oxidation	190.8	398.4	531.4	517.5	6.0	1.1
650 °C annealing	191.4	399.0	532.7	516.9	5.0	1.0

The UPS spectral width is ~15.2 eV, indicating that BN-2 exhibits an NEA.[27]

The measured binding energies of the B 1s, N 1s, O 1s, and V $2p_{3/2}$ core levels, the work function, and the VBM for BN-2 are summarized in Table III.

D. BN-3

Spectroscopic results from sample BN-3 are shown in Fig. 4. Compared with BN-2, a thicker 0.5 nm vanadium film was deposited on O-terminated c-BN and compared with BN-2. After annealing, the V $2p_{3/2}$ peaks were detected with stronger intensity at 513.2 eV and 515.3 eV. Observing the V $2p_{3/2}$ core level at 515.3 eV has been suggested to indicate V_2O_3.[31] Moreover, 513.2 eV corresponds to the core level of metallic vanadium, indicating there was excess vanadium that was not fully involved in forming V-O bonds. The O 1s peak was detected at 531.4 eV, 1.3 eV lower than that in samples BN-1 and BN-2, implying a larger contribution of vanadium oxide to the oxides on the c-BN surface compared with BN-1 and BN-2. In addition, the back cutoff of the UPS spectrum was at the same position as sample BN-2. However, the front cutoff was at the position of the Fermi level, within the experimental uncertainty, indicating metallic surface character, which is attributed to either metallic vanadium or the metallic phase of V_2O_3.
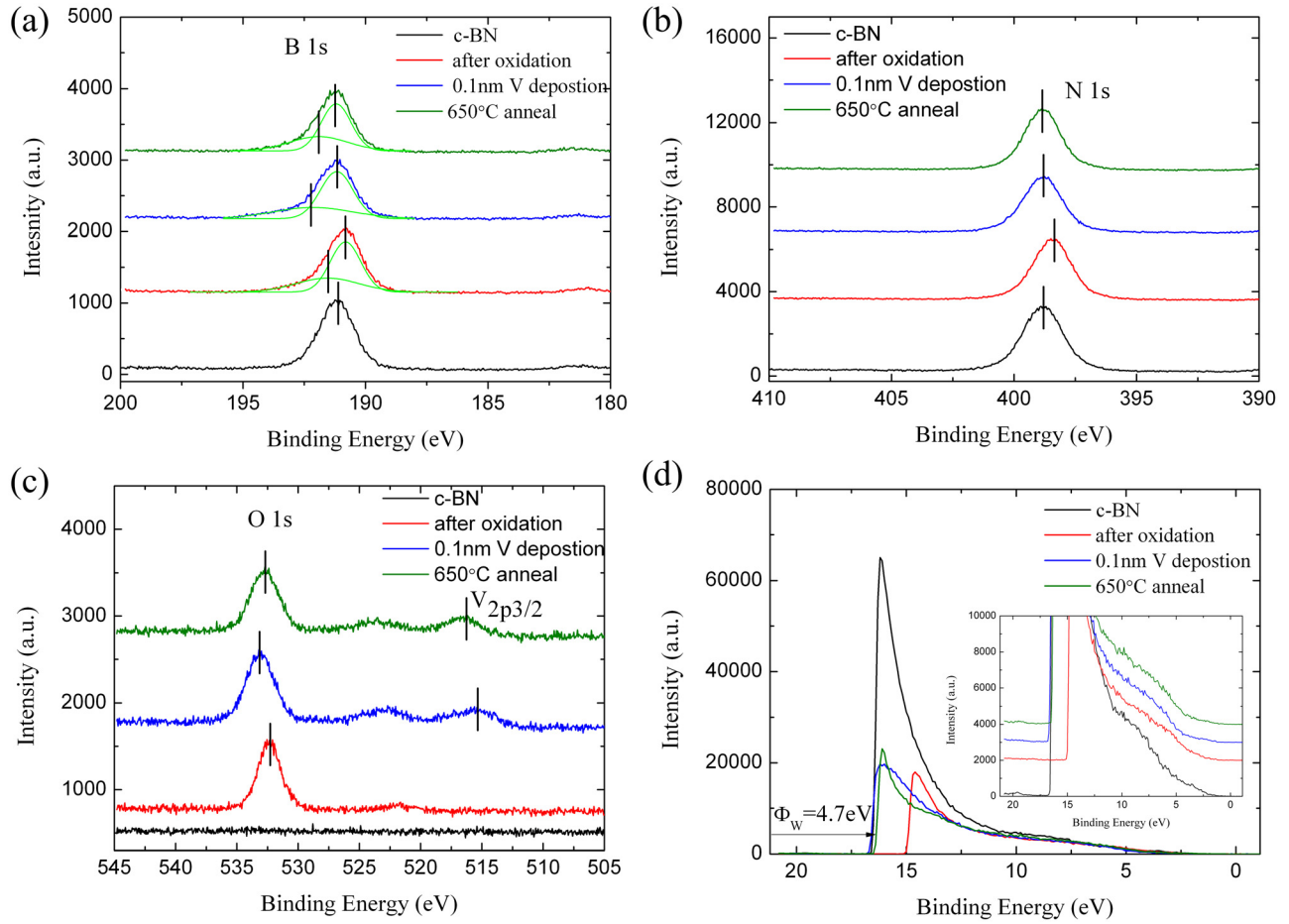
FIG. 3. XPS scans of BN-2, showing the (a) B 1s, (b) N 1s, (c) O 1s and V 2p$_{3/2}$ core level peaks, and (d) the UPS scans.

The measured binding energies of the B 1s, N 1s, O 1s, and V 2p$_{3/2}$, core levels, the work function, and the VBM for BN-3 are summarized in Table IV.

IV. DISCUSSION

A. Surface and interface composition

Previous research indicated that boron nitride films synthesized by ECR-PECVD employing fluorine chemistry are composed of hexagonal BN (h-BN) near the substrate and c-BN on the surface.[32] An absence of a π-plasmon peak in the XPS B 1s and N 1s spectra indicates that h-BN is not detected and c-BN predominates at the sample surface.

It is necessary to determine the specific atoms bonded to oxygen, after oxidation of the c-BN films. In Fig. 3(a), a shoulder is observed at 193.2 eV near the B 1s core level main peak, which is close to the B 1s core level in B$_2$O$_3$.[31]

TABLE III. B 1s, N 1s, O 1s, V 2p$_{3/2}$ core levels, effective work function (Φ$_W$), and VBM for BN-2 relative to the Fermi level, in eV.

Process	B 1s	N 1s	O 1s	V 2p$_{3/2}$	Φw	VBM
H-termination	191.2	398.8	…	…	4.6	1.5
Oxidation	190.8	398.4	532.3	…	6.2	1.8
Vanadium deposition	191.2	398.8	533.1	515.7	4.5	1.1
650 °C annealing	191.2	398.8	532.7	516.6	4.7	1.3

Additionally, the O 1s peak is located at 532.7 eV, which is close to the reported binding energy of B-O bands.[31] In contrast, no distinguishable N-O shoulder was evident around the N 1s main peak after the oxygen plasma process. The surface B:N atomic ratios can be estimated from an XPS stoichiometry analysis. In this case, the B:N atomic ratio can be approximately calculated using the following equation:

$$B:N\,atomic\,ratio = \frac{I_B/S_B}{I_N/S_N},\qquad(1)$$

where I_B and I_N are the integrated intensities of the B 1s and N 1s peaks from Figs. 3(a) and 3(b). The S_B and S_N are the atomic sensitivity factors for the B 1s and N 1s peaks, which are 0.159 and 0.477, respectively.[33] The B:N atomic ratio of the surface increased ∼4% after oxidation, indicating that nitrogen atoms were removed during the oxidation process. Therefore, the oxygen atoms tended to bond with boron to form B-O bonds at the c-BN surface.

The amount of vanadium covering the surface of the sample is estimated from the XPS spectra using the following equation:[34]

$$\Theta_V = \frac{I_V}{S_V}\bigg/\left(\frac{I_B}{S_B}+\frac{I_N}{S_N}\right)*\sum_{n=0}^{\infty}\exp\left[\frac{-n*d_{BN}}{\lambda_{BN}*\cos(\varphi)}\right],\quad(2)$$

where Θ_V, the coverage in monolayers (ML), is the number of absorbed V atoms per unit area (atoms/cm^2) divided by
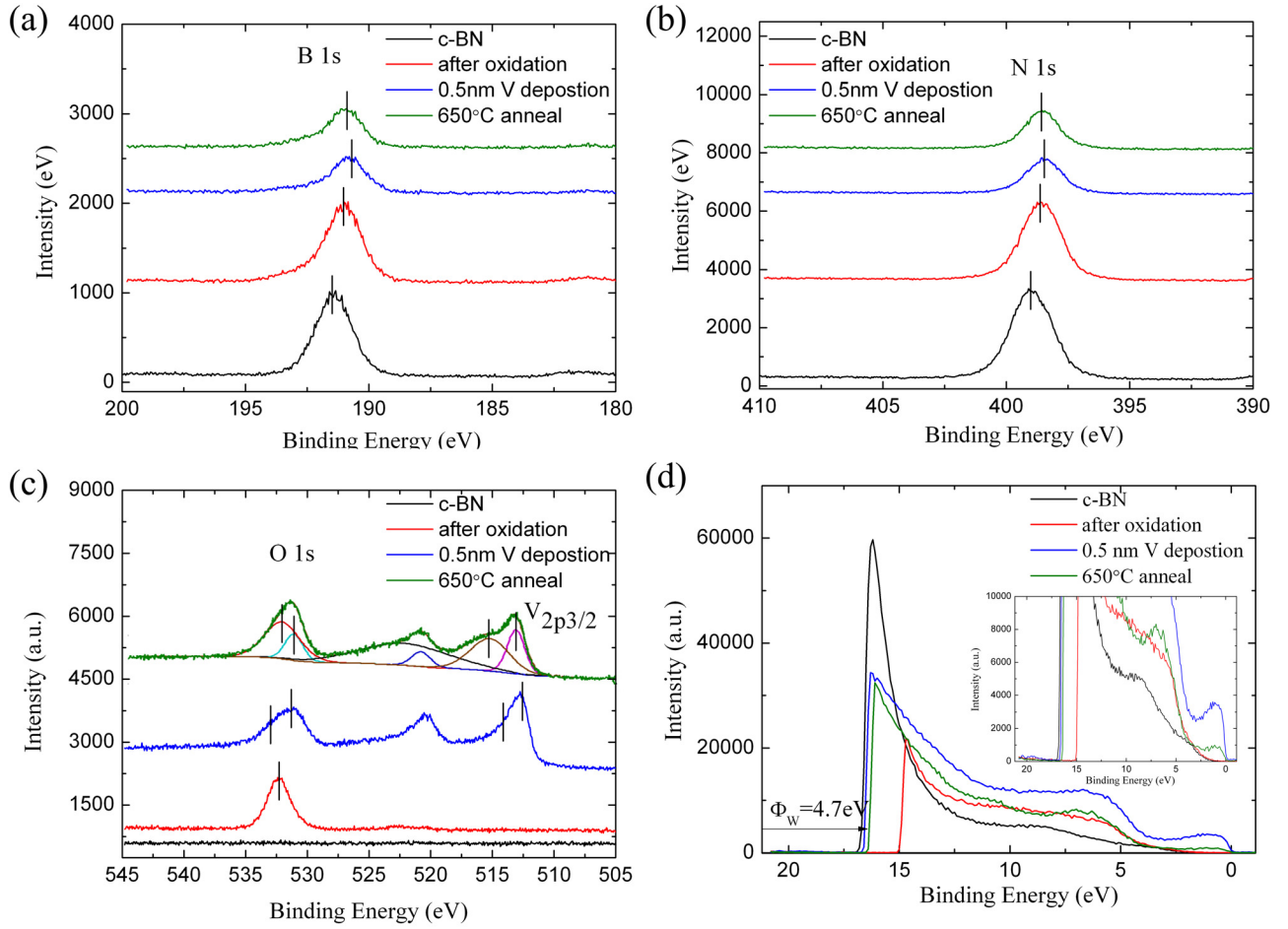
FIG. 4. XPS scans of BN-3, showing the (a) B 1s, (b) N 1s, (c) O 1s and V 2p$_{3/2}$ core level peaks, and (d) the UPS scans.

the number of B and N atoms per unit area (atoms/cm^2) on the surface. I_V, I_B, and I_N are the integrated intensities of the V 2p$_{3/2}$, B 1s, and N 1s peaks from Fig. 1(c). The S_V, S_B, and S_N are the atomic sensitivity factors for the V 2p$_{3/2}$, B 1s, and N 1s photoelectrons; d_{BN} is the average spacing between *c*-BN planes, which is 1.28 Å, where we assume polycrystalline c-BN surface is comprised of ⟨100⟩, ⟨110⟩, and ⟨111⟩ planes; $\lambda_{BN} \approx 31.6$ Å (Ref. 9) is the inelastic mean free path of electrons in c-BN, which is approximated by the average of the inelastic mean free paths of B 1s and N 1s electrons; φ is the angle between the normal direction and the XPS energy analyzer, which is 0° for this setup. The vanadium coverage on the c-BN surface was calculated to be ∼0.26 ML. The coverage of oxygen on the c-BN surface can be similarly calculated using Equation (2), and after annealing it was found to be ∼3.0 ML.

TABLE IV. B 1s, N 1s, O 1s, V 2p$_{3/2}$ core levels, effective work function (Φ_W), and VBM for BN-3 relative to the Fermi level, in eV.

Process	B 1s	N 1s	O 1s	V 2p$_{3/2}$	Φ_W	VBM
H-termination	191.4	399.0	…	…	4.3	1.8
Oxidation	191.0	398.6	532.5	…	6.1	1.9
Vanadium deposition	190.8	398.5	531.5/534.0	512.7/514.1	4.5	−0.2
650 °C annealing	190.9	398.6	531.4/533.0	513.2/515.3	4.7	−0.1

Here, we consider that the oxide on the c-BN samples is composed of B$_2$O$_3$ and vanadium oxides. For the BN-1 sample, after annealing, the V 2p$_{3/2}$ core level was 516.9 eV, which has been suggested to indicate the presence of VO$_2$.[31] Here, we have taken into account an ∼0.8 eV downward band bending that resulted from photo-induced charging. Considering the relative amount of vanadium and oxygen, VO$_2$ is calculated to contribute ∼24% of the oxide on the c-BN surface, and the remaining oxide is B$_2$O$_3$. For BN-2, with the same amount of vanadium deposited on the O-terminated c-BN surface, the vanadium coverage was calculated to be ∼0.39 ML using Equation (2), and the oxygen coverage is ∼3.3 ML. After annealing, the V 2p$_{3/2}$ core level was 516.6 eV, which indicates VO$_2$.[31] The VO$_2$ accounted for ∼31% of the oxide on the c-BN surface. A similar composition of oxides formed on the c-BN surface while controlling the amount of vanadium deposited. It appears that B$_2$O$_3$ is always formed regardless of the oxidation process sequence, which may be explained by the lower enthalpy of formation of B$_2$O$_3$ ($\Delta H_{B2O3} = -1273$ cal/mol, $\Delta H_{VO2} = -713$ cal/mol).

For BN-3, with 0.5 nm vanadium deposited onto the O-terminated c-BN, after annealing the V 2p$_{3/2}$ core level was observed at 516.6 eV, which corresponds to V$_2$O$_3$.[31] In this case, the O 1s peak can be resolved into components for B$_2$O$_3$ and V$_2$O$_3$. The composition of the oxide was estimated by fitting the O 1s peak, which is shown in Fig. 4(c). The

V_2O_3 accounted for $\sim$26% of the oxide on the c-BN surface. The vanadium film was not completely oxidized. However, consistent with results of BN-1 and BN-2, a fraction ($\sim$30%) of sites with V-O-termination is apparently sufficient to change the electron affinity of the surface.

B. Plasma and annealing effects

The results indicate a decrease in binding energy of the core levels after oxygen plasma treatment, which suggests upward band bending. It is likely that the oxygen plasma process introduces a concentration of defects or interstitial oxygen atoms, which act as electron traps or acceptors. A prior study on transition-metal oxides (TiO_2, ZrO_2, and HfO_2) suggested that oxygen can diffuse into the transition metal oxide layer during plasma processing, and the excess oxygen can be removed by vacuum annealing to $\sim$550 °C.[35] These defects are compensated by ionized impurities or defects in the c-BN films, resulting in a negatively charged layer in the oxide and a positively charged layer in the c-BN. This dipole layer results in an outward directed electrical field, which leads to upward band bending.

Annealing is apparently able to eliminate this kind of upward band bending presumably by removing the defects or interstitial oxygen atoms in the oxide. Since the oxide layer is at the surface, the O 1s peak is expected to shift more than the B 1s and N 1s peaks. For example, in O-terminated c-BN, the B and N core levels shifted $\sim$0.6 eV to lower binding energy after oxygen plasma treatment. Annealing restored the B and N 1s peaks, while the O 1s peak shifted $\sim$0.7 eV in the same direction.

C. Electronic properties

Two models, namely, the interface barrier model and the surface dipole model, have been suggested to describe the mechanism of inducing an NEA by metal or metal oxide thin films.[36,37] The band schematics of the two models are shown in Fig. 5. For the interface barrier model, if the c-BN surface is coated with a thin layer of metal or metal oxide, the vacuum level for this thin layer will effectively describe the electron affinity and potentially enable electron emission into vacuum. If the vacuum level of the surface oxide layer lies beneath the CBM of c-BN, an NEA is achieved on the surface. The surface dipole model considers that the metal-oxide bonds at the c-BN surface form a layer of dipoles that creates a surface electrical field. If the dipole is directed

away from the surface, the vacuum level can be shifted to a position lower than the CBM, leading to an NEA.

The vanadium-oxide-terminated c-BN films exhibit an NEA, regardless of the sequence, whether introducing vanadium first followed by oxidization, or vice versa. One possible explanation is that the vanadium-oxide dipoles on the c-BN films act as a metal-oxide layer. The configuration is described by two interfaces, the semiconductor/metal-oxide interface and the metal-oxide/vacuum interface. The thin oxide layer introduces an energy barrier at the oxide/c-BN interface, lowering the electron emission threshold and resulting in an NEA surface condition. The effect of the metal-oxide layer is apparently independent of how this layer is formed. Another possibility is that, in the annealing process, the vanadium and oxygen atoms were activated for diffusion, and structural changes occurred at the surface of c-BN films. The same surface dipole layer could be formed after annealing, leading to a similar state of the surface.

During the oxidation of vanadium, a layer of B_2O_3 is introduced adjoining the c-BN. When the c-BN surface is terminated with B_2O_3, the surface exhibits a PEA. According to the surface dipole model, it appears that the B_2O_3 acts as an acceptor layer on the c-BN surface and is compensated by a positively charged layer at the c-BN surfaces. This charge transfer can be explained by the difference of the electronegativities of the two atoms ($X_B = 2.04$, $X_O = 3.44$ (Ref. [28])). This dipole layer results in an outward electrical field, which shifts the vacuum level to a higher position, leading to a PEA. According to previous studies, hydrogen atoms are mostly involved in N-H bonds, promoting an NEA.[9] Comparing O-terminated c-BN with H-terminated c-BN, the surface dipoles, which determine the electron affinity of c-BN surfaces, changed from N-H to B-O. During the oxidation process, not only the surface termination atoms changed but also the active surface atoms of the c-BN changed. The change of the surface dipole leads to the change of the electron affinity.

In contrast with O-terminated c-BN, the vanadium-oxide termination leads to an NEA, indicating that the vanadium-oxide layer can act as a donor layer. According to the data of BN-2, the B 1s and N1s core levels of c-BN were not affected by the annealing process. The binding energy is the same as that of H-terminated c-BN, indicating there is essentially no band bending in c-BN introduced by VO_2 and B_2O_3. In this model, the charges are at the interface of B_2O_3 and VO_2. Therefore, VO_2 on a B_2O_3 terminated c-BN surface changes the surface dipole from the O-terminated c-BN. The negative charge in the B_2O_3 layer is not balanced by an ionized layer in c-BN, but by the positive charge in the VO_2 layer. A thin VO_2 layer on the B_2O_3 terminated c-BN surface forms a B-O-V structure, which introduces an inward electric field and results in a reduction of the work function. The changes of the vacuum level due to the surface dipoles are shown in Fig. 6 and are similar to the model presented for GaAs surfaces, which showed an effective NEA activated by (Cs, O) layers.[16]

Although the results presented here establish an NEA for the VO_2 terminated surfaces, the value of the NEA and the value of the work function, which are both important for
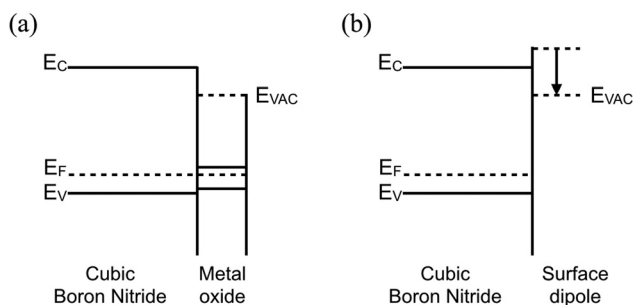

FIG. 5. Band schematics of the two models: (a) interface barrier model and (b) surface dipole model.
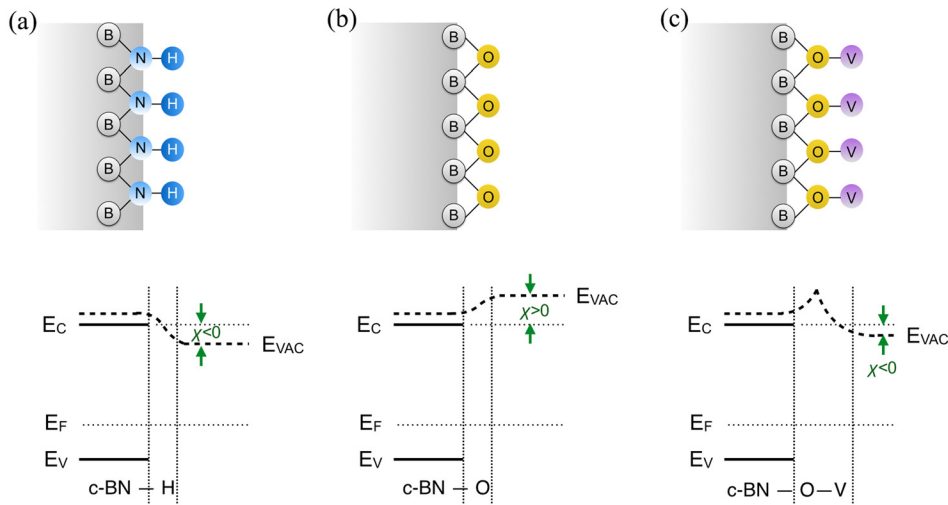
FIG. 6. Schematic diagrams of surface dipoles and corresponding band diagrams for (a) H-terminated c-BN, (b) O-terminated c-BN, and (c) vanadium-oxide-terminated c-BN. The changes of the vacuum level due to surface dipoles are profiled.
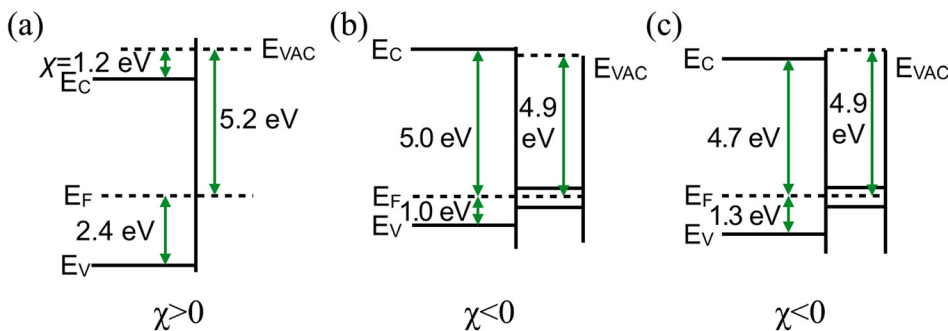

FIG. 7. Band schematics near the c-BN surface of (a) O-terminated c-BN, (b) BN-1, and (c) BN-2.

electron emission, cannot be directly determined from these photoemission measurements. To determine these values, it is necessary to locate the position of the vacuum level within the bandgap, but this was not possible in these measurements since emission was not detected from states below the CBM. To approximate the value of the NEA, a reported value of the work function of VO_2, 4.9 eV,[38] is used. Combined with the measured values of the CBM positions, a 0.1 eV NEA on BN-1 and a small PEA $\sim$ 0.2 eV on BN-2 would be expected. In these two cases, the emission barrier is nearly zero for electrons approaching the surface at the CBM. The discrepancy between the spectral results and the calculated results may result from the fact that the actual work function of this thin VO_2 layer varies from the reported value due to its very small thickness. The band diagram configurations in the region close to the c-BN surface for O-terminated c-BN, BN-1, and BN-2 are illustrated in Fig. 7. The shifts of the position of the Fermi level within the c-BN band gap for the different configurations are attributed to band bending, which occur in the film beyond the region indicated in the figure.

V. CONCLUSION

Thin layers of vanadium-oxide were formed on c-BN surfaces, and the resulting electronic structure was examined by *in-situ* XPS and UPS. An NEA was observed on the vanadium-oxide-terminated c-BN sample, while the O-terminated c-BN without vanadium showed a PEA. We propose that the B_2O_3 layer is favorable for the formation of the B-O-V layer

structure, which provides a thermally stable surface dipole. The results show that the surface condition (i.e., work function and electron affinity) of c-BN can be modified in a controlled way by careful choice of metal-oxide-termination. The results also indicated that a thermally stable NEA surface on c-BN could be achieved through vanadium-oxide-termination, which leads to possible applications in energy conversion devices.

ACKNOWLEDGMENTS

[1]F. J. Himpsel, J. A. Knapp, J. A. VanVechten, and D. E. Eastman, Phys. Rev. B **20**, 624 (1979).
[2]B. B. Pate, Surf. Sci. **165**, 83 (1986).
[3]J. van der Weide, Z. Zhang, P. K. Baumann, M. G. Wensell, J. Bernholc, and R. J. Nemanich, Phys. Rev. B **50**, 5803 (1994).
[4]F. A. M. Koeck and R. J. Nemanich, Diamond Relat. Mater. **18**, 232–234 (2009).
[5]F. A. M. Koeck, R. J. Nemanich, A. Lazea, and K. Haenen, Diamond Relat. Mater. **18**, 789 (2009).
[6]T. Sun, F. A. M. Koeck, A. Rezikyan, M. M. J. Treacy, and R. J. Nemanich, Phys. Rev. B **90**, 121302(R) (2014).
[7]C. B. Samantaray and R. N. Singh, Int. Mater. Rev. **50**, 313 (2005).
[8]R. M. Chrenko, Solid State Commun. **14**, 511 (1974).
[9]J. Shammas, T. Sun, F. A. M. Koeck, A. Rezikyan, and R. J. Nemanich, Diamond Relat. Mater. **56**, 13 (2015).

[10]M. J. Powers, M. C. Benjamin, L. M. Porter, R. J. Nemanich, R. F. Davis, J. J. Cuomo, G. L. Doll, and S. J. Harris, Appl. Phys. Lett. **67**, 3912 (1995).

[11]K. P. Loh, K. Nishitani-Gamo, I. Sakaguchi, T. Taniguchi, and T. Ando, Appl. Phys. Lett. **72**, 3023 (1998).

[12]K. P. Loh, I. Sakaguchi, M. Nishitani-Gamo, T. Taniguchi, and T. Ando, Diamond Relat. Mater. **8**, 781 (1999).

[13]M. I. Landstrass and K. V. Ravi, Appl. Phys. Lett. **55**, 975 (1989).

[14]H. Nakahata, T. Imai, and N. Fujimori, in *Proceedings of 2nd International Symposium on Diamond Material* (1991), p. 487.

[15]S. Ri, C. E. Nebel, D. Takeuchi, B. Rezek, N. Tokuda, S. Yamasaki, and H. Okushi, Diamond Relat. Mater. **15**, 692 (2006).

[16]C. Y. Su, W. E. Spicer, and I. Lindau, J. Appl. Phys. **54**, 1413 (1983).

[17]K. P. Loh, X. N. Xie, S. W. Yang, J. S. Pan, and P. Wu, Diamond Relat. Mater. **11**, 1379 (2002).

[18]C. Bandis, D. Haggerty, and B. B. Pate, Mater. Res. Soc. Symp. Proc. **339**, 75 (1994).

[19]K. M. O'Donnell, M. T. Edmonds, J. Ristein, A. Tadich, L. Thomsen, Q.-H. Wu, C. I. Pakes, and L. Ley, Adv. Funct. Mater. **23**, 5608 (2013).

[20]K. M. O'Donnell, T. L. Martin, M. T. Edmonds, A. Tadich, L. Thomsen, J. Ristein, C. I. Pakes, N. A. Fox, and L. Ley, Phys. Status Solidi A **211**, 2209 (2014).

[21]A. K. Tiwari, J. P. Goss, P. R. Briddon, A. B. Horsfall, N. G. Wright, R. Jones, and M. J. Rayson, Europhys. Lett. **108**, 46005 (2014).

[22]C. N. Berglund and H. J. Guggenheim, Phys. Rev. **185**, 1022 (1969).

[23]F. J. Morin, Phys. Rev. Lett. **3**, 34 (1959).

[24]K. Kosuge, J. Phys. Chem. Solids **28**, 1613 (1967).

[25]T. Sun, "Combined photo- and thermionic electron emission from low work function diamond films," Ph.D. dissertation (ProQuest/UMI, Arizona State University, Ann Arbor, 2013), Publication No. AAT 3605487.

[26]X. Gouin, P. Grange, L. Bois, P. L'Haridon, and Y. Laurent, J. Alloys Compd. **224**, 22 (1995).

[27]R. J. Nemanich, P. K. Baumann, M. C. Benjamin, S. W. King, J. van der Weide, and R. F. Davis, Diamond Relat. Mater. **5**, 790 (1996).

[28]W. M. Haynes, *CRC Handbook of Chemistry and Physics*, 94th ed. (CRC Press, Boca Raton, 2013–2014).

[29]K. E. Smith and V. E. Henrich, Surf. Sci. **225**, 47 (1990).

[30]P. Baumann and R. J. Nemanich, Surf. Sci. **409**, 320 (1998).

[31]S. Surnev, M. G. Ramsey, and F. P. Netzer, Prog. Surf. Sci. **73**, 117 (2003).

[32]W. J. Zhang, S. Matsumoto, K. Kurashima, and Y. Bando, Diamond Relat. Mater. **10**, 1881 (2001).

[33]Casa Software Ltd., "CasaXPS Manual 2.3.15 Spectroscopy," Pressed by Casa Software Ltd.

[34]V. M. Bermudez, J. Appl. Phys. **80**, 1190 (1996).

[35]C. C. Fulton, G. Lucovsky, and R. J. Nemanich, Appl. Phys. Lett. **84**, 580 (2004).

[36]P. K. Baumann, S. P. Bozeman, B. L. Ward, and R. J. Nemanich, Diamond Relat. Mater. **6**, 398 (1997).

[37]K. M. O'Donnell, T. L. Martin, N. A. Fox, and D. Cherns, Phys. Rev. B **82**, 115303 (2010).

[38]C. Zhu, M. Kaur, F. Tang, X. Liu, D. J. Smith, and R. J. Nemanich, J. Appl. Phys. **112**, 084105 (2012).